

ORIGINAL RESEARCH ARTICLE

Transient receptor potential channel-related biomarkers for prognostic assessment in hepatocellular carcinoma

Dong Chen¹, Jun Yin¹, Chao Yang¹, Bo Li², and Jing Li^{3*}

¹Department of General Surgery, Shanxi Bethune Hospital, Taiyuan, Shanxi, China

²Department of Anesthesiology, The Fourth Hospital of Shijiazhuang, Shijiazhuang, Hebei, China

³Central Operating Department, Shanxi Bethune Hospital, Taiyuan, Shanxi, China

Abstract

Hepatocellular carcinoma (HCC) is the most common and fatal form of liver cancer and has been associated with the transient receptor potential channel (TRPC) family. However, the exact mechanism underlying this connection remains elusive. In this study, we aimed to investigate the role of TRPCs in HCC using bioinformatics methods. We employed bioinformatics methods to screen and determine the biomarkers (cytochrome P450 family 2 subfamily C member [CYP2C9], kinesin family member 20A [KIF20A], secreted phosphoprotein 1 [SPP1], and TMF-regulated nuclear protein 1 [TRNP1]) for the risk score of HCC patients. To further verify our findings, we conducted western blotting to determine the expression levels of these biomarkers in HCC and normal samples. Functional characterization of the corresponding genes was conducted through wound healing, cell counting kit-8, and transwell invasion assays using cell lines with gene knockdown or overexpression. Notably, there were significant differences in the levels of 13 types of immune cells between the two risk groups, such as activated dendritic cells and activated CD4⁺ T cells. Western blotting indicated that KIF20A, SPP1, and TRNP1 were upregulated in HCC, which is consistent with the differential analysis. In the TRNP1 overexpression group, the cell migration distance, cell viability, and cell invasion ability were enhanced. In conclusion, this study identified four biomarkers, namely CYP2C9, KIF20A, SPP1, and TRNP1, and established a risk model for HCC. Our findings can pave the way for improving the diagnosis and treatment options for HCC using TRPC-related biomarkers.

*Corresponding author:

Jing Li
(lj245515933@163.com)

Citation: Chen D, Yin J, Yang C, Li B, Li J. Transient receptor potential channel-related biomarkers for prognostic assessment in hepatocellular carcinoma. *Cancer Plus*. 2026;8(2):4858. doi: 10.36922/cp.4858

Received: September 14, 2024

Revised: March 6, 2025

Accepted: April 7, 2025

Published online: June 16, 2025

Copyright: © 2025 Author(s). This is an Open-Access article distributed under the terms of the Creative Commons Attribution License, permitting distribution, and reproduction in any medium, provided the original work is properly cited.

Publisher's Note: AccScience Publishing remains neutral with regard to jurisdictional claims in published maps and institutional affiliations.

Keywords: Hepatocellular carcinoma; Transient receptor potential; Differentially expressed genes; Consensus clustering analysis; Risk score

1. Introduction

Liver cancer is the fourth leading cause of cancer-related deaths globally and ranks sixth in incidence worldwide.^{1,2} Hepatocellular carcinoma (HCC), which constitutes the primary histological subtype, accounts for roughly 90% of all liver cancer cases.^{3,4} Men are more predisposed to developing HCC than women,⁵ and the incidence rates vary widely among countries, with Asia reporting the highest caseload.⁶ Patients diagnosed with liver cancer often face early metastasis and a poor prognosis. The 5-year survival

rate for liver cancer is merely 18%.⁷ The incidence rate of liver cancer among individuals aged 20 – 39 ranks fourth globally, with an age-standardized incidence rate of 29.0 cases per 100,000 individuals.⁸ HCC remains the dominant histological subtype of primary liver cancer. Notably, nearly 75 – 85% of HCC patients have a history of chronic hepatitis B or C virus infection.^{9,10} Metastasis and post-surgical recurrence are two pivotal factors that significantly impact HCC mortality.¹¹ A recent study revealed that approximately 90% of HCC-related deaths can be attributed to metastases.¹²

At present, the approaches to treating HCC exhibit diversified characteristics, encompassing surgeries, chemotherapy, radiotherapy, liver transplantations, targeted therapy, and immunotherapy, all of which play a pivotal role in HCC management.¹³ In the realm of immunotherapy, immune checkpoint inhibitors have emerged as a significant modality for liver cancer treatment. For patients with low Radiomic Immunoscore, they benefit more from anti-PD-1 immunotherapy. Therefore, for those patients, receiving anti-PD-1 immunotherapy after surgery might improve the prognosis.¹⁴ Turning to traditional Chinese medicine for liver cancer treatment, it emphasizes a holistic approach and syndrome differentiation in its treatment principles. Herbs such as astragalus and ginseng can bolster the body's immune system and elevate its defenses against tumors. Furthermore, certain traditional Chinese medicine components, such as curcumin, have demonstrated promising anti-liver cancer properties, capable of inhibiting the growth, spread, and invasion of liver cancer cells.¹⁵ In the field of gene therapy, technologies such as clustered, regularly interspaced short palindromic repeats-associated protein 9 can be employed to edit liver cancer-related genes. This holds the potential to rectify aberrant gene expression or mend mutated genes, ultimately aiming to treat liver cancer. In addition, gene therapy encompasses the construction of gene vectors to deliver therapeutic genes into liver cancer cells. For instance, introducing tumor suppressor genes can effectively curb the proliferation and metastasis of liver cancer cells.¹⁶

Nonetheless, even with these treatment methods, it is still challenging to completely eradicate HCC. Patients remain at risk of the cancer spreading to other tissues or organs even after receiving treatment. For patients diagnosed with very early or early-stage HCC, the currently available primary treatment options include surgical resection, ablation, and transplantation.¹³ However, many patients are unable to undergo these interventions due to the regional disease progression or metastasis.¹⁷

HCC is a highly aggressive cancer with a generally poor prognosis, significantly impacting the survival rates and

quality of life for those affected. Furthermore, it poses a significant threat to public health.¹⁸ Given these detrimental effects, there is an urgent need to explore the underlying mechanisms of HCC development. This research is vital for establishing theoretical foundations that can lead to better clinical outcomes and the development of more effective treatment strategies.

The transient receptor potential (TRP) channels (TRPCs) are transmembrane proteins that, upon activation, permit the passage of cations, such as calcium ions, across the membrane.¹⁹ These channel proteins play a crucial role in regulating sensorimotor signaling both within multicellular organisms and at the cellular level.²⁰ Within cells, calcium ions exercise direct control over tumor cell proliferation, invasion, metastasis, and differentiation.²¹ Notably, rapidly proliferating tumor cells frequently exhibit elevated levels of calcium ions.²² TRPCs' dysfunctions, such as abnormal expression, intracellular relocation, or mutations, have been linked to various diseases. As a result, TRPC dysfunction has been associated with tumors of the digestive tract.²³

The TRPC family primarily encompasses TRPC1, TRPC5, TRPC6, TRP vanilloid 1, TRP melastatin (TRPM) 2, TRPM6, TRPM7, and TRPM8.^{24,25} Notably, TRPC6 expression is elevated in HCC tissues and is associated with the progression of HCC. When stimulated by transforming growth factor-beta, TRPC6 and the sodium-calcium exchanger (NCX1) increase in abundance, forming the TRPC6/NCX1 complex. This complex facilitates the migration, invasion, and intrahepatic metastasis of HCC cells induced by transforming growth factor-beta, suggesting that TRPC6 and NCX1 could be promising targets for the treatment of HCC.²⁶ Furthermore, Xu *et al.*²⁷ have uncovered that TRPC6 and TRP vanilloid 6 are pivotal channels that are overexpressed in HCC cells.

However, the majority of existing studies focus on the TRPC family genes. Notably, TRPC-related genes (TRPGs), which are not directly involved in encoding TRPC proteins, play crucial roles in the function or regulation of TRPCs. Our current understanding of TRPGs in HCC remains relatively limited, and there are scarce bioinformatics studies exploring TRPCs in this context. Therefore, conducting a comprehensive and systematic bioinformatics study on genes related to the TRP pathway in HCC can offer a fresh perspective and theoretical foundation for predicting prognostic markers of this disease.

In this study, we developed a prognostic model centered around TRPCs to improve clinical risk stratification for HCC patients. This has profound implications for guiding management decisions and predicting patient

outcomes. In addition, we explored the prognostic characteristics to understand how TRPCs impact the tumor microenvironment. Furthermore, we assessed the prognostic importance of TRPGs and examined their effects on the tumor microenvironment, response to immune checkpoints, and drug sensitivity.

2. Data and methods

2.1. Data collection

RNA sequencing (RNA-seq) data and somatic mutation data of The Cancer Genome Atlas (TCGA)-Liver HCC Collection, including 374 HCC and 50 normal healthy samples, were sourced from the TCGA database (<http://portal.gdc.cancer.gov/>). Of these, 368 HCC samples consisted of survival and clinical information and were used as a training set (Table S1). Furthermore, the RNA-seq expression matrix of the International Cancer Genome Consortium (ICGC)-LIRI, including 205 normal healthy and 240 HCC samples with survival information, was acquired from the ICGC database (<https://dcc.icgc.org/>). In addition, the background gene set for “Reactome_TRP_channels” was obtained from the Molecular Signatures Database (MSigDB) (<http://www.gsea-msigdb.org/gsea/msigdb>). Meanwhile, the gene set for the “inflammatory mediator regulation of TRP channels” pathway was acquired from the Kyoto Encyclopedia of Genes and Genomes (KEGG) database (<https://www.kegg.jp/entry/ko04750>). After deduplication and merging, a total of 107 TRPGs were identified.²⁸ All data were accessed and downloaded in October 2022.

2.2. Differential analysis of differentially expressed TRPGs (DE-TRPGs)

DE-TRPGs between the normal and HCC samples were obtained using the R package “limma” (version 3.5.1) with adjusted $p < 0.05$ and $|\log_2 \text{fold change [FC]}| > 0.5$.²⁹ The result was visualized through a volcano plot, box plot, and heatmap using the R package “ggplot2” (version 3.3.2) and “heatmap” (version 0.7.7).³⁰ Subsequently, the R package “maftools” (version 2.2.10) was applied to analyze the DE-TRPG mutation frequencies in the HCC samples. The result was visualized using a waterfall plot. In addition, a protein–protein interaction (PPI) network was generated.

2.3. Candidate gene screening

Consensus clustering analysis was conducted based on the DE-TRPGs using the R package “ConsensusClusterPlus” (version 1.54.0) to divide the samples into different clusters.³¹ Consequently, Kaplan–Meier (K–M) analysis was performed to compare the survival probability among clusters. A Chi-square test was conducted to determine the percentage of patients with different clinical features

(neoplasm histologic grade, pathologic N, or pathologic T). Subsequently, differentially expressed genes (DEGs) among the clusters and between the normal and HCC samples were determined using the R package “limma” with adjusted $p < 0.05$ and $|\log_2 \text{FC}| > 1$.²⁹ Finally, an intersection between the two types of DEGs was conducted to identify the candidate genes.

2.4. Constructing the HCC risk model

First, a univariate Cox analysis was performed to identify the candidate genes with a survival correlation based on the training (368 TCGA samples of HCC) and validation (240 ICGC samples of HCC) sets with survival data. The least absolute shrinkage and selection operator (LASSO) algorithm was applied to filter these genes. Second, the multivariate Cox analysis was performed to identify biomarkers based on the genes persisting after using the LASSO algorithm. We calculated the risk scores based on the following formula in Equation I,

$$\text{risk score} = \alpha_1 \times X_1 + \alpha_2 \times X_2 + \dots + \alpha_n \times X_n \quad (\text{I})$$

where α is the regression coefficient. The hazard ratio value can be obtained after considering its anti-log. Finally, samples in these data sets were separated into risk groups based on the median risk scores. The receiver operating characteristic (ROC) and K–M analyses were conducted, and a principal component analysis (PCA) was performed to detect the distribution pattern of the risk groups.

2.5. Risk model analysis by independent prognostic analysis

The clinical features (pathologic N, pathologic M, pathologic T, neoplasm histologic grade, age, and gender) and risk score were analyzed using the univariate and multivariate Cox analyses. The Wilcoxon test was performed to detect significant differences in risk scores between the sub-stages in clinical features and overall survival (OS). Next, the single-sample gene set enrichment analysis (ssGSEA) was conducted, depending on the gene sets acquired from the MSigDB database, to obtain the pathway scores for each sample (<http://www.gsea-msigdb.org/gsea/msigdb>). Based on the $|\text{difference score}| > 2$ and adjusted $p < 0.05$, we visualized the Hallmark and KEGG pathways using heatmaps.

2.6. Enrichment and immune analyses between the risk groups

First, DEGs between the risk groups were obtained using the R package “limma” with adjusted $p < 0.05$ and $|\log_2 \text{FC}| > 1$.²⁹ The “DAVID” tool was used for the DEG enrichment analysis based on the gene ontology (GO) and KEGG database.³² Second, the gene set enrichment analysis software (version 4.0.3) was applied to enrich

the GO-biological process (GO-BP) functions and KEGG pathways of the risk groups.

Based on the training set, the ESTIMATE algorithm was used to compare the tumor purity, stromal score, ESTIMATE score, and immune score between the risk groups. Subsequently, the ssGSEA algorithm was applied to compare the immune cells between the risk groups. Finally, correlations between the differential existence of immune cells and biomarkers were calculated.

2.7. Western blotting

After obtaining consent, five patients with HCC were recruited from the Shanxi Bethune Hospital. HCC and cancer-adjacent tissues were collected from these patients. The patients' ages ranged from 59 to 68 years old, with an average age of 63 ± 4.50 years. The specific information is shown in Table S2. Radioimmunoprecipitation assay lysis buffer (Beyotime, China) was used for cell lysis and protein extraction. The bicinchoninic acid assay protein quantification kit (Beyotime, China) was used to measure the protein concentration. Protein samples were separated using sodium dodecyl sulfate-polyacrylamide gel electrophoresis and then transferred to a polyvinylidene fluoride membrane. The polyvinylidene fluoride membrane was first blocked with skim milk at room temperature for 30 min and then incubated with the primary antibody overnight at 4°C. After incubation, the membrane was washed with Tris-buffered saline Tween-20 solution. Subsequently, the membrane was incubated with the secondary antibody horseradish peroxidase-conjugated goat anti-rabbit immunoglobulin G at room temperature for 30 min and then washed again with Tris-buffered saline Tween-20 solution. Finally, the expression of target proteins was detected by the enhanced chemiluminescence chemiluminescent system, and the results were analyzed using Image J software (64-bit Java 8).

2.8. Real-time quantitative polymerase chain reaction (RT-qPCR)

Total RNA was extracted using the FastPure Complex Tissue/Cell Total RNA Isolation Kit (Vazyme, China). The ABScript III RT Master Mix for RT-qPCR with gDNA Remover (ABclonal, China) was used for reverse transcription. Subsequently, RT-qPCR was performed using the Genius $\times 2$ SYBR Green Fast RT-qPCR Mix (ABclonal, China). During the data analysis phase, the $2^{-\Delta\Delta C_t}$ method was employed with *GAPDH* as the endogenous control. The primer sequences were as follows:

- (i) TMF-regulated nuclear protein 1 (*TRNP1*): Forward: GCCCAGTAGAGGAGGCTGAG
Reverse: ACGTCTTCCTGAAGGCAGTG.
- (ii) *GAPDH*: Forward: GGAGTCCACTGGCGTCTTCA
Reverse: GTCATGAGTCCTTCCACGATACC.

2.9. Construction of knockdown and overexpression cell lines

Human HCC cell HuH-7 was purchased from Xiamen Immocell Biotechnology Co., Ltd (China). The cells were cultured in a complete medium containing 90% Dulbecco's Modified Eagle's Medium, 10% fetal bovine serum, and penicillin-streptomycin and were routinely maintained in an incubator at 37°C with 5% carbon dioxide and 95% air.

Total RNA was extracted from HuH-7 cells, and the complementary DNA of *TRNP1* was obtained through reverse transcription. Subsequently, *TRNP1* was amplified using PCR using specific primers with the following sequences: *TRNP1*-Forward: ATTCCTCGAGGCCACCATGCCGGGCTGCCG CATCAGC and *TRNP1*-Reverse: GCCGCTCTAGATC AGCGCTGCGGGGAGGC. The obtained complementary DNA fragment was cloned into the pLVX overexpression lentiviral vector containing XhoI and XbaI restriction sites. In addition, the small hairpin (sh) RNA-seqs targeting *TRNP1* were as follows: sh*TRNP1*-1: TGTCATTGCT TCAAGTCTAAC, sh*TRNP1*-2: CCTGAGATGCAAT CAGATTAA, and sh*TRNP1*-3: AGATATCGTCATCA TTCTTAA. These sequences were cloned into the pLKO.1 vector and packaged to generate lentiviral particles. Subsequently, these lentiviruses were used to transfect HuH-7 cells, and stable cell lines were obtained through selection with 2 $\mu\text{g/mL}$ puromycin. Finally, the expression levels of *TRNP1* in the overexpressing or knockdown cell lines were detected using RT-qPCR and western blot.

2.10. Wound healing assay

HuH-7 cells were seeded in 6-well plates (6×10^4 cells per well) and cultured for 24 h in an incubator at 37°C with 5% carbon dioxide. Subsequently, a scratch was made in the wells of the 6-well plate using a 200 μL pipette tip. The cells were then washed thrice with phosphate-buffered saline to remove the cells dislodged during the scratching process, followed by the addition of a serum-free medium. Then, photographs of the scratched areas were taken using an inverted microscope (MSHOT, China), and the percentage of cell migration area was calculated.

2.11. Cell counting kit-8 assay

HuH-7 cells were seeded into 96-well plates for culture. At different time points (0, 24, 48, and 72 h), 10 μL of the cell counting kit-8 assay solution (Servicebio, China) was added to each well. Subsequently, the cells were incubated in the cell culture incubator for 30 min, and the absorbance (OD) values of each well were measured at 450 nm.

2.12. Transwell invasion assay

Cells in good growth conditions were harvested and incubated in a serum-free medium for 24 h to induce starvation. Subsequently, Matrigel (Corning, United States) and serum-free medium were diluted in a ratio of 1:8 and mixed thoroughly. A volume of 60 μ L of the mixture was added to the Transwell chamber and incubated at 37°C for 3 h, after which the unbound matrix gel was aspirated. The chamber was then hydrated with serum-free culture medium for 30 min and was checked to ensure that no liquid had passed through the chamber. The samples were then prepared with serum-free medium, and the Transwell chamber was placed into a 24-well plate. The cells were digested and seeded into the upper chamber at a density of 40,000 cells per well. The 24-well plate was then incubated at 37°C, with 5% carbon dioxide and 90% humidity for 24–48 h. The Transwell chamber was subsequently removed, and a 4% paraformaldehyde fixative was added for 30 min. After washing with phosphate-buffered saline, 1% crystal violet staining solution was added for 20 min for staining, followed by three washes with phosphate-buffered saline. The chamber was air-dried and then observed and photographed under a microscope (MSHOT, China). Quantitative analysis was performed by counting the cells with ImageJ software (64-bit Java 8) and calculating the average value.

3. Results

3.1. DE-TRPGs between normal and HCC samples

We acquired 16 DE-TRPGs between normal and HCC samples using a differential analysis (Figure 1A and B) (Table S3). The heatmap presents the DE-TRPG expression for each sample (Figure 1C). We identified *TRPM8* was the most frequent mutation, predominantly a missense mutation (Figure 1D and E). PPI network analysis resulted in a total of 192 predicted relationship pairs. Among them, *ADCY3* demonstrated the maximum correlations with genes such as *ADCY4*, *GNAS*, and *ADCY1* (Figure 1F).

3.2. Consensus clustering and differential analyses

In the consensus clustering analysis, the *K* index value was determined to be two according to the cumulative distribution function (Figure 2A and B). Based on the *K* index, the samples were divided into two clusters. The survival probability of Cluster 2 was significantly different from that of Cluster 1 (Figure 2C and D). In addition, we observed significant differences in four clinical features (age, gender, OS, and neoplasm histologic grade) between the clusters (Figure 2E–I). Next, we obtained 346 DEGs between the clusters and 1,415 DEGs between the healthy and HCC samples using differential analyses (Figure 3A–D) (Tables S4 and S5). Finally, we performed an intersection

between the two types of DEGs and obtained 220 candidate genes (Figure 3E).

3.3. Hepatocellular carcinoma risk model consisting of four biomarkers

We performed the univariate Cox analysis to identify 97 candidate genes with a survival correlation, and the forest plot depicts four of these genes (Figure 4A). The optimal lambda value of the LASSO algorithm was selected based on the minimum criterion to filter relevant genes. As a result, 11 genes, including *ADH4*, *ANXA10*, *CFHR3*, cytochrome P450 family 2 subfamily C member (*CYP2C9*), *ETV4*, *FTCD*, *G6PD*, kinesin family member 20A (*KIF20A*), secreted phosphoprotein 1 (*SPP1*), *TPX2*, and *TRNP1*, were ultimately retained (Figure 4B and C). After the multivariate Cox analysis, four biomarkers (*CYP269*, *KIF20A*, *SPP1*, and *TRNP1*) were identified, and the risk scores were calculated (Figure 4D). We separated the samples (training and validation sets) into two risk groups (Figure 4E and F). The high-risk group demonstrated a worse survival probability than the low-risk group (Figure 5A and B). Eventually, both values of the area under the ROC curve suggested that the risk model displayed a preferable prognostic prediction performance of HCC (Figure 5C and D). In addition, we conducted PCA between the risk groups based on the two sets. The sample distributions were remarkably different between the high- and low-risk groups (Figure 5E and F).

3.4. Identification of two independent prognostic factors

Two clinical features, including the pathologic T and M and risk scores, were identified through the univariate Cox analysis (Figure 6A). Results of the multivariate Cox analysis suggested that risk scores and pathologic T were the independent prognostic factors (Figure 6B). Subsequently, risk scores between the sub-stages in OS, pathologic T, and neoplasm histologic grade demonstrated a significant difference (Figure 6C–E). The heatmap depicts the expression of biomarkers in each sample (Figure 6F). In addition, the ssGSEA results demonstrated 33 hallmark pathways, including spermatogenesis and G2/M checkpoint, and 132 KEGG pathways, including linoleic acid metabolism and peroxisome, between normal and HCC samples (Figure 6G and H). Tables S6 and S7 show the total enrichment information.

3.5. Enrichment and immune analyses of the risk model

We obtained 352 DEGs between the risk groups using differential analysis (Figure 7A and B) (Table S8). These DEGs were enriched in 179 GO-BP functions, such as

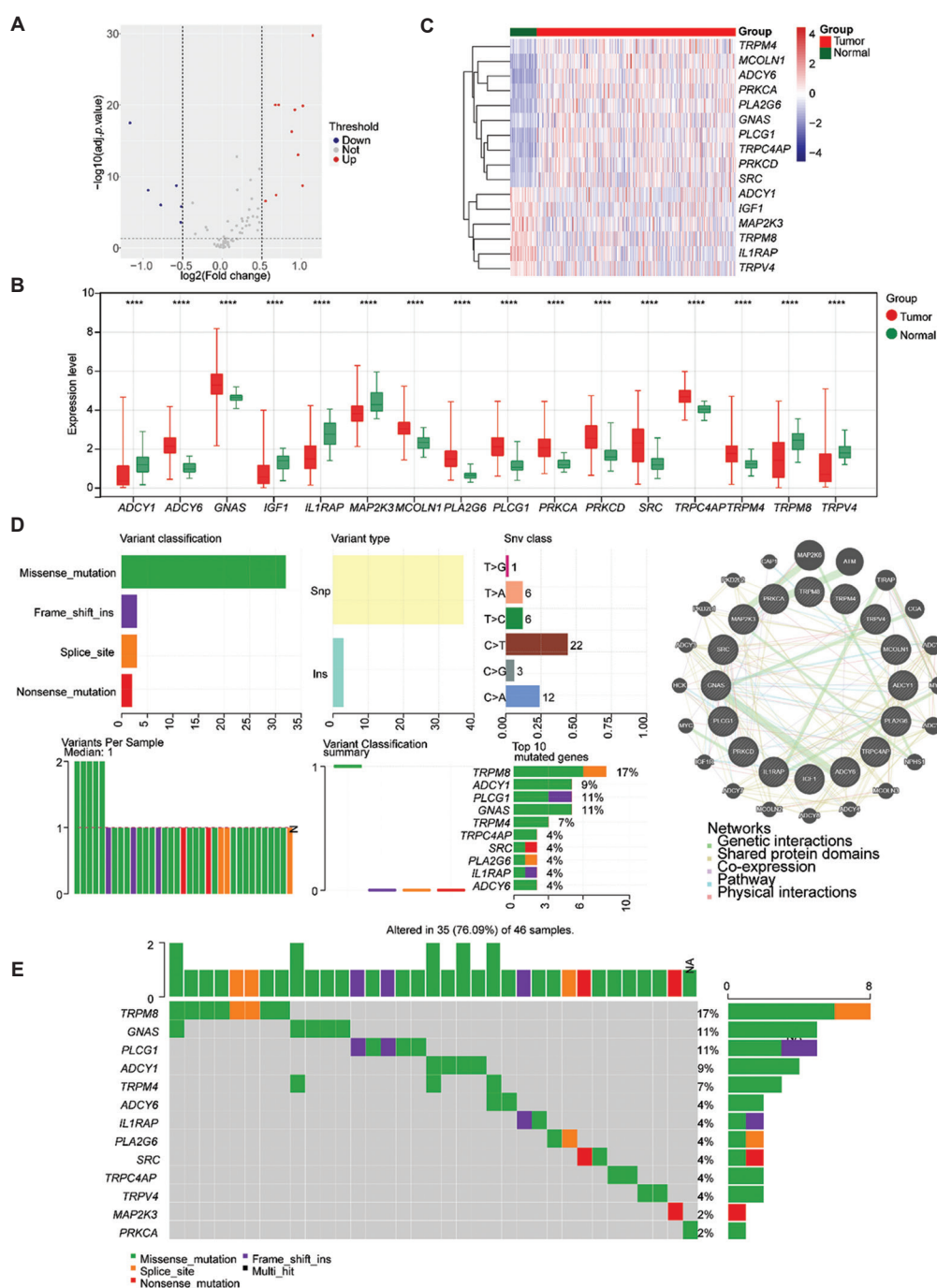


Figure 1. Identification of the differentially expressed transient receptor potential channel-related genes (DE-TRPGs). (A) Volcano map of DE-TRPGs. A dot represents a gene, red dots represent genes with upregulated expression, blue dots represent genes with downregulated expression, and gray dots represent genes with non-significant expression differences. (B) Box plot of DE-TRPGs expression. Red represents tumor samples, and green represents normal samples, using the Benjamini–Hochberg method for multiple test correction. (C) Heatmap of 16 DE-TRPGs between healthy and HCC samples in the TCGA-HCC dataset. Each small square represents a gene, and its color indicates the expression level of the gene. The higher the expression level, the darker the color (red indicates high expression, and blue indicates low expression). (D) Overview of mutations in the TCGA-HCC cohort. (E) Waterfall plot of specific DE-TRPG mutation profiling in HCC samples. Bar graphs indicate the frequencies of the different mutation types. (F) PPI network of DE-TRPGs using GeneMANIA. Different colored lines represent different bioinformatics methods.

Note: **** represents adjusted $p < 0.0001$.

Abbreviations: HCC: Hepatocellular carcinoma; Ins: Insertion; PPI: Protein-protein interaction; SNP: Single nucleotide polymorphism; SNV: Single nucleotide variation; TCGA: The Cancer Genome Atlas.

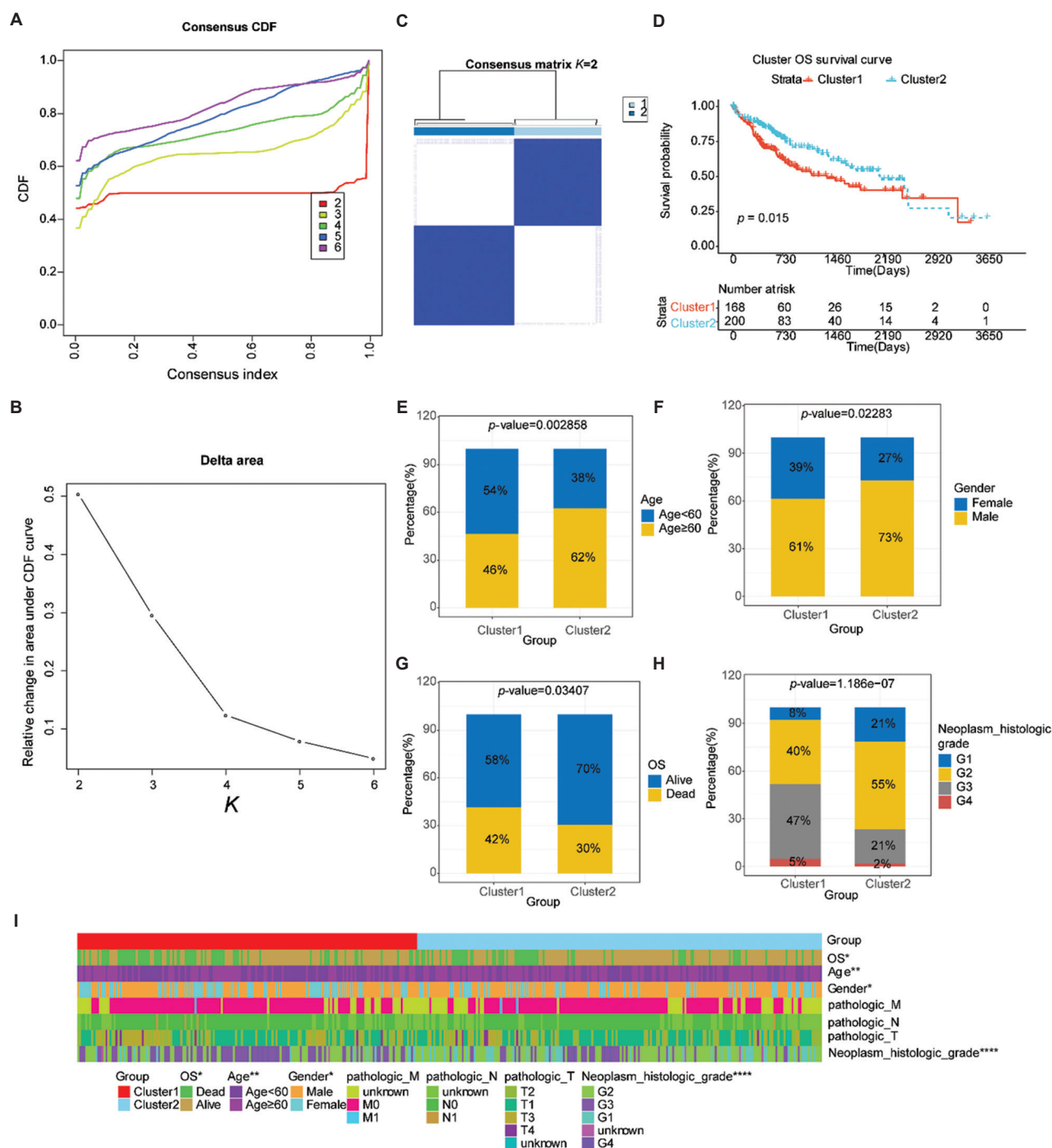


Figure 2. Consensus clustering to identify the two clusters of hepatocellular carcinoma samples based on the differentially expressed transient receptor potential channels-related genes. (A) CDF curve of $K = 2 - 6$. (B) Relative change in area under the CDF curve for $K = 2 - 6$. (C) Consensus heatmaps for $K = 2$ display a relatively stable partitioning of the samples. (D) Survival analysis of different clusters ($p=0.015$). Bar chart for the distribution of the TCGA-HCC cohort with different clinical features, including the (E) age, (F) gender, (G) OS, and (H) neoplasm histologic grade, screening clinical features with significant differences using the Chi-square test. (I) Heatmap for the clinical feature ratios between two clusters. Each row represents a clinical feature, and different colors represent different subtypes.

Notes: * indicates $p<0.05$; ** indicates $p<0.01$; *** indicates $p<0.001$; **** indicates $p<0.0001$.

Abbreviations: CDF: Cumulative distribution function; HCC: Hepatocellular carcinoma; OS: Overall survival; TCGA: The Cancer Genome Atlas.

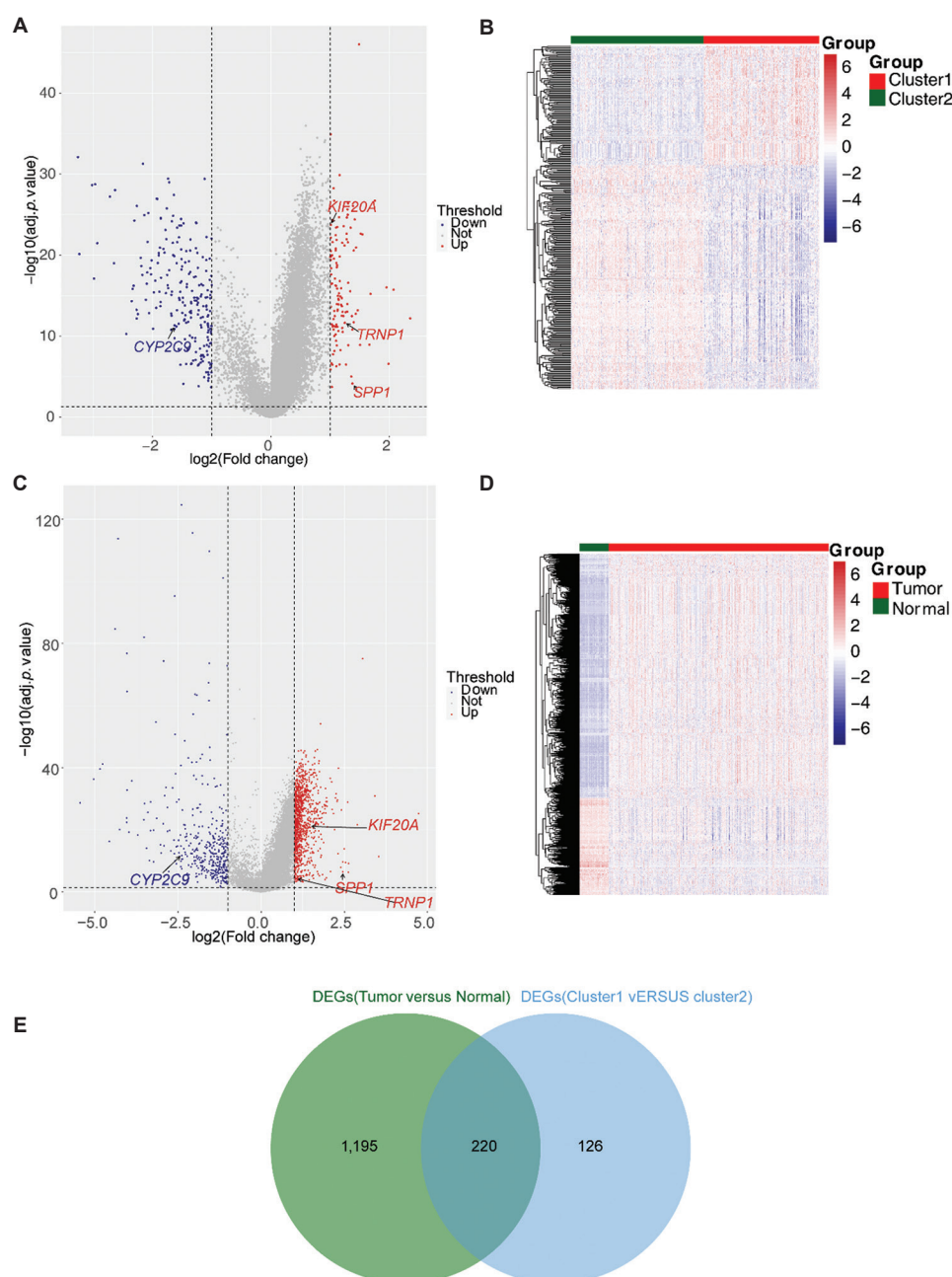


Figure 3. Differential expression analysis for the candidate genes. (A) Volcanic map of differentially expressed genes (DEGs) between Clusters 1 and 2. The red dots indicate upregulated genes, the blue dots indicate downregulated gene expression levels, and the gray dots indicate no significant differences in gene expression. (B) Heat map of DEGs expression between Clusters 1 and 2. Each small square represents a gene, and its color indicates the expression level of that gene. The higher the expression level, the darker the color (red represents high expression and blue represents low expression). The left tree diagram represents the clustering analysis results of different genes in different samples. (C) Volcanic map of DEGs between hepatocellular carcinoma (HCC) and control samples. (D) Heat map of DEGs expression between HCC and control samples. The volcano map and heatmap were both calibrated using the Benjamini–Hochberg method for multiple tests, with a difference threshold set at adjusted $p < 0.05$ and $|\log_2 \text{fold change}| > 1$. (E) Venn diagram for 220 candidate genes that are common with the DEGs from different sources.

xenobiotic and drug metabolic processes, 47 GO-cellular component functions, such as lipid metabolic process and extracellular exosome, 78 GO-molecular functions, such as intracellular membrane-bounded organelle and

monooxygenase activity (Figure 7C), and 40 KEGG pathways, such as metabolic pathways and the xenobiotic metabolism by cytochrome P450 (Figure 7D). In addition, we detected the top five GO-BP functions and KEGG

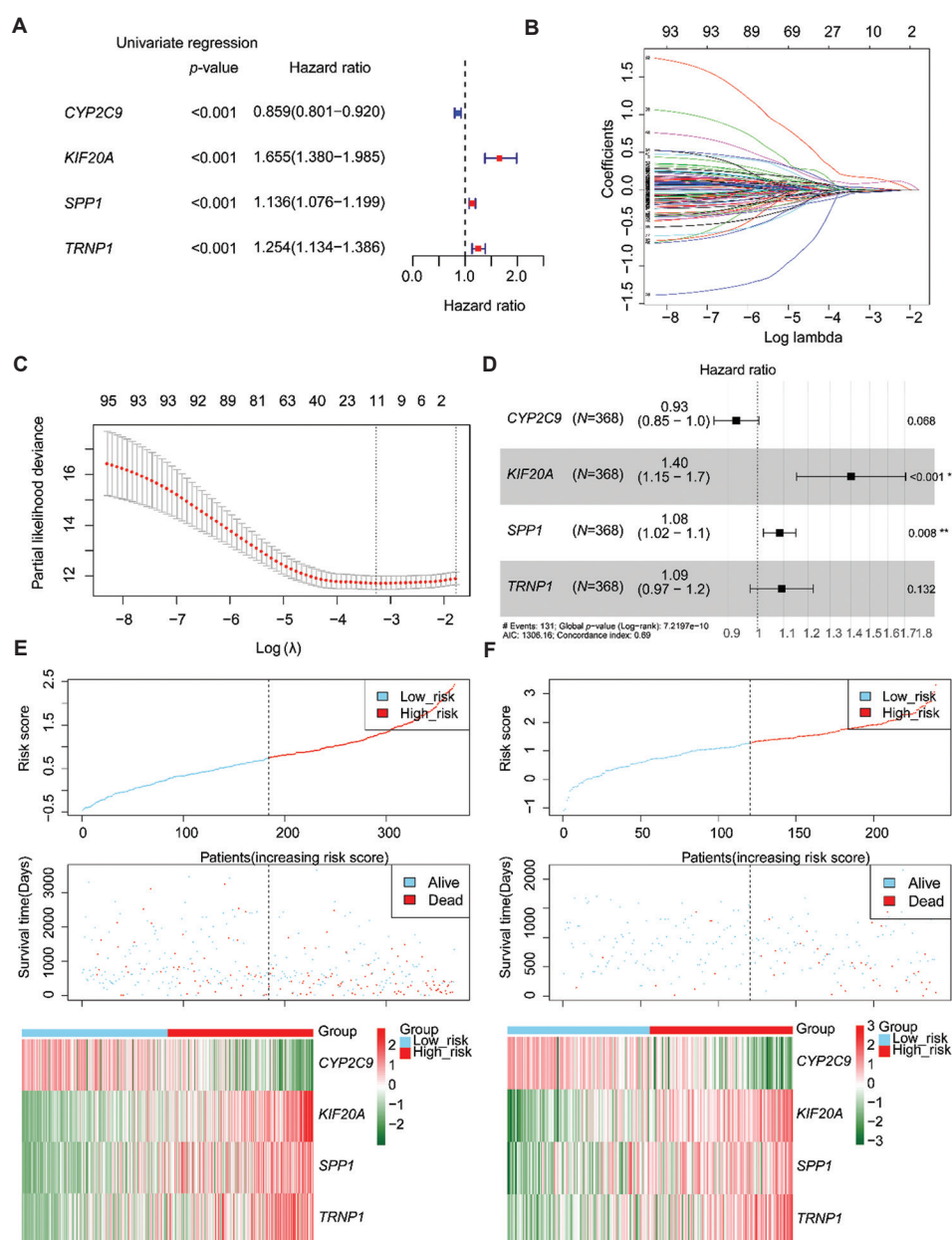


Figure 4. Constructing the prognostic risk model for hepatocellular carcinoma (HCC). (A) Forest plot for the univariate Cox analysis. The left side represents genes and their corresponding p -values and hazard ratio (HR) values. The red square on the right indicates HR value >1 , and the blue square indicates HR value <1 . The line segments on both sides of the square represent the 95% confidence interval of the HR value. (B) Non-zero characteristic gene coefficient map. (C) Lambda (λ) selection diagram in the least absolute shrinkage and selection operator model. Two dashed lines represent two special values of λ , with λ minimum on the left and λ least-square estimation on the right. λ minimum had higher accuracy and used more genes. (D) Forest plot of multivariate Cox analysis. The left side represents genes and corresponding sample sizes and HR values. The black square on the right indicates that the HR value is less than or greater than 1 and the corresponding p -value. The line segments on both sides of the square represent the 95% confidence interval of the HR value. Risk curve and heatmap of high and low-risk groups of the (E) TCGA-HCC dataset and the (F) ICGC-HCC dataset. Notes: ** indicates $p < 0.01$; *** indicates $p < 0.001$.

Abbreviations: ICGC: International Cancer Genome Consortium; TCGA: The Cancer Genome Atlas.

pathways with the highest correlation with the risk groups. The high-risk group was significantly enriched in Gene Ontology Biological Process (GO-BP) functions, such as the nucleotide sugar metabolic process and cell cycle

process (Figure 8A), as well as in Kyoto Encyclopedia of Genes and Genomes (KEGG) pathways, including the cell cycle and purine metabolism (Figure 8B). The low-risk group was enriched in GO-BP functions, such as the

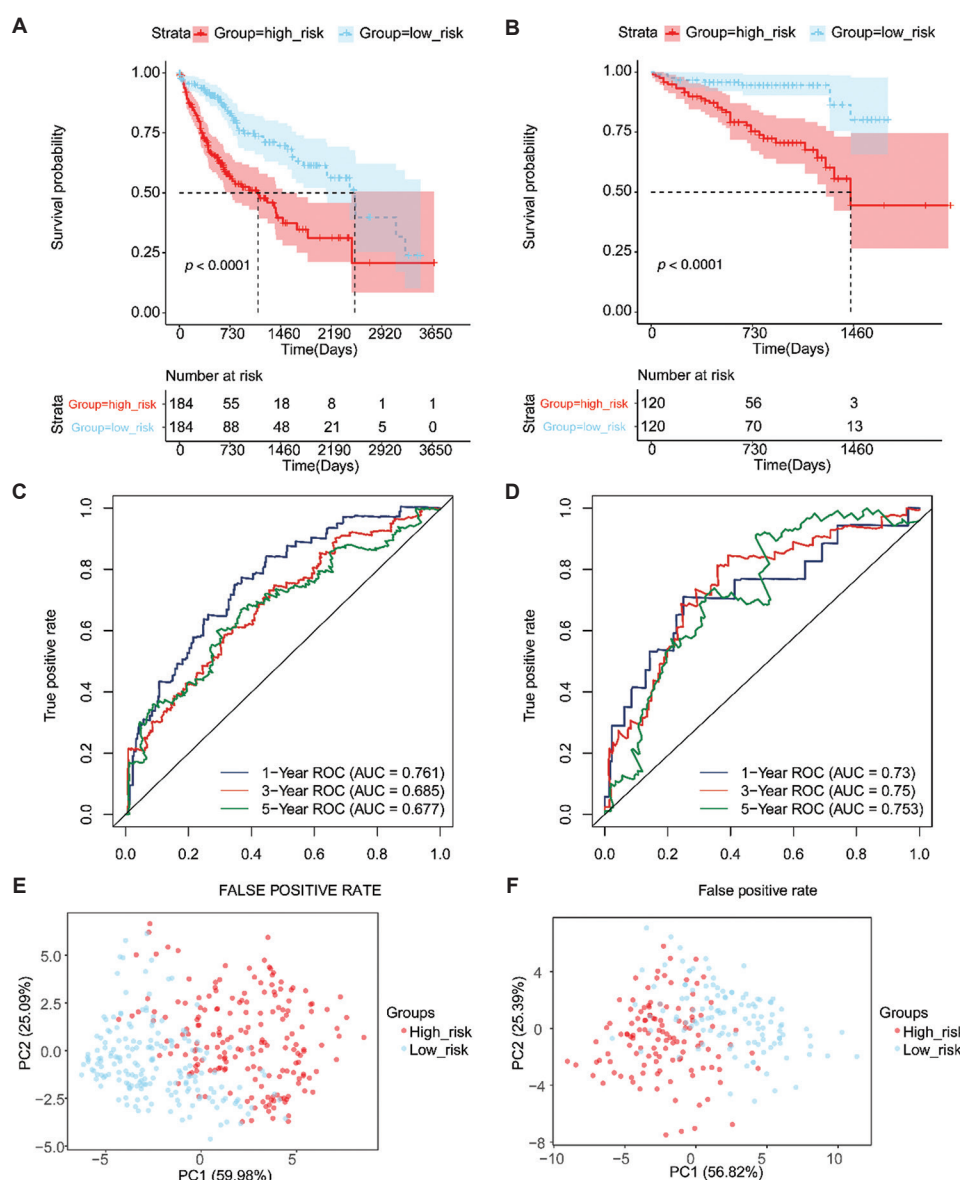


Figure 5. Exploring the predictive performance of the risk model in patients with hepatocellular carcinoma (HCC). Kaplan–Meier curves of different risk groups using (A) TCGA-HCC ($p < 0.0001$) dataset and (B) ICGC-HCC ($p < 0.0001$) dataset. The red curve represents the high-risk group, and the blue curve represents the low-risk group. ROC curves of the prognostic model for survival prediction of patients at 1, 3, and 5 years using (C) TCGA-HCC dataset and (D) ICGC-HCC dataset. PCA chart of patients in high and low-risk groups using (E) TCGA-HCC dataset and (F) ICGC-HCC dataset.

Abbreviations: AUC: Area under the curve; ICGC: International cancer genome consortium; PCA: Principal component analysis; ROC: Receiver operating characteristic; TCGA: The Cancer Genome Atlas.

epoxygenase p450 pathway and 2-oxoglutarate metabolic process (Figure 8C), and KEGG pathways, such as fatty acid metabolism and primary bile acid biosynthesis (Figure 8D).

The immune score was substantially higher in the high-risk group than in the low-risk group (Figure 9A). We identified 13 types of immune cells, including activated dendritic cells and activated CD4 T cells, which were significantly different between the risk groups (Figure 9B).

The *KIF20A* biomarker demonstrated the strongest positive and negative correlations with activated CD4 T cells and eosinophils, respectively (Figure 9C).

3.6. Enhanced migration distance, viability, and invasion ability of cells in the *TRNP1* overexpression group

Although the potential biomarkers identified through bioinformatics analysis provide valuable insights for

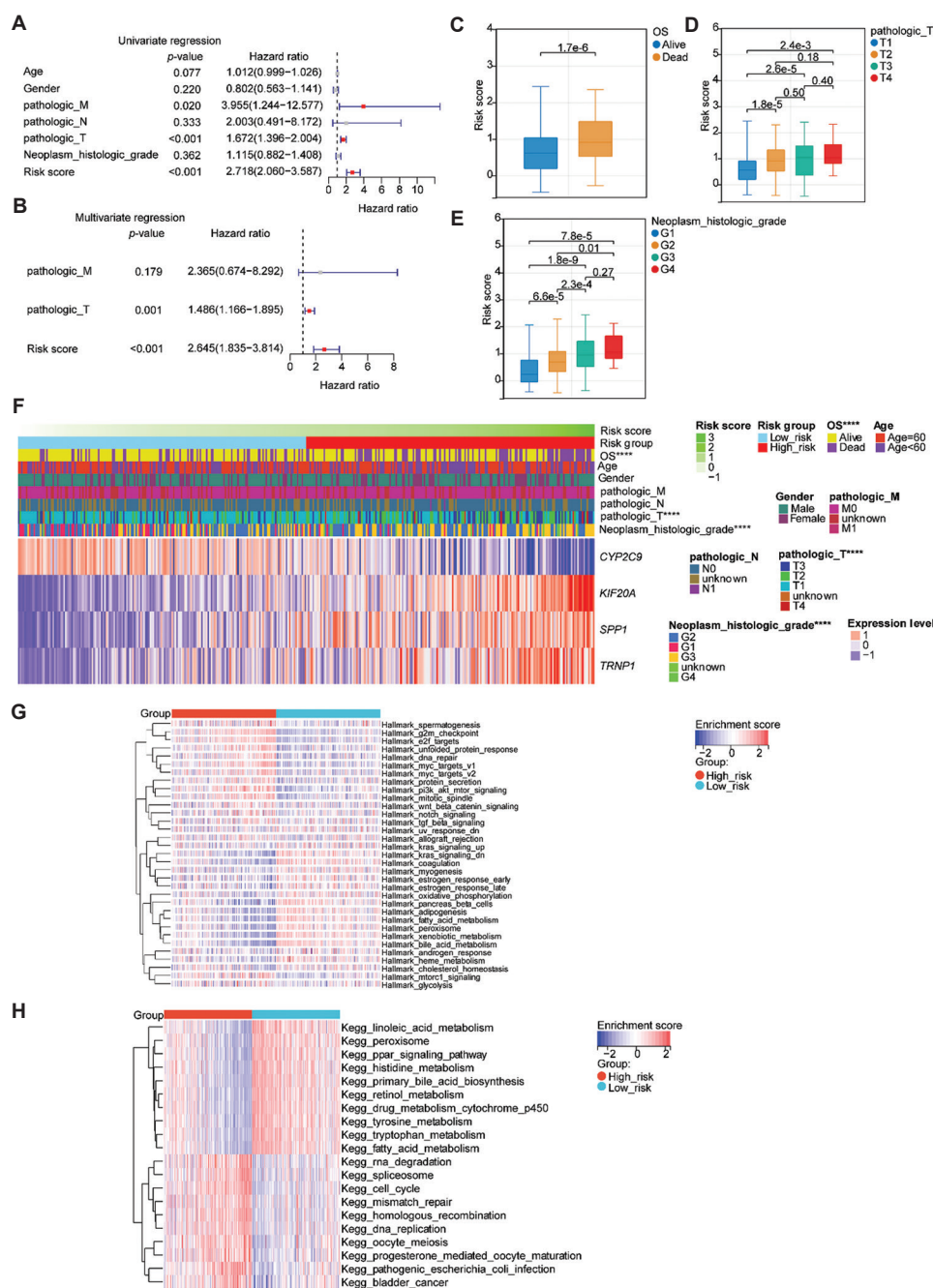


Figure 6. Clinical correlation analysis of risk scores. (A) Forest plot for the independent prognostic-univariate Cox analysis. (B) Forest plot for the independent prognostic multivariate Cox analysis. The left side represents clinical features and corresponding p -values and hazard ratio (HR) values. The red square on the right represents an HR value >1 , and the line segments on both sides of the square represent the 95% confidence interval of the HR value. The gray square represents a $p>0.05$, indicating that the feature is not significant. Box plots for the risk score of patients with hepatocellular carcinoma in different clinical subgroups, including (C) overall survival (OS) sub-stages, (D) pathologic tumor (T), and (E) neoplasm histologic grade. Differential analysis was conducted using the Wilcoxon test method. (F) Heat map of biomarker expression between high-risk groups and different clinical features. (G) Hallmark enrichment heatmap of differences between sample groups. (H) Kyoto Encyclopedia of Genes and Genomes enrichment heatmap of differences between sample groups using the Benjamini-Hochberg method for multiple test correction, and the difference threshold was set at adjusted $p<0.05$ and $|\text{score}|>2$. Note: **** indicates $p<0.0001$.

disease diagnosis and treatment, their exact roles and biological significance cannot be fully confirmed based

solely on computational results. Therefore, it is necessary to further validate and deeply explore them through a

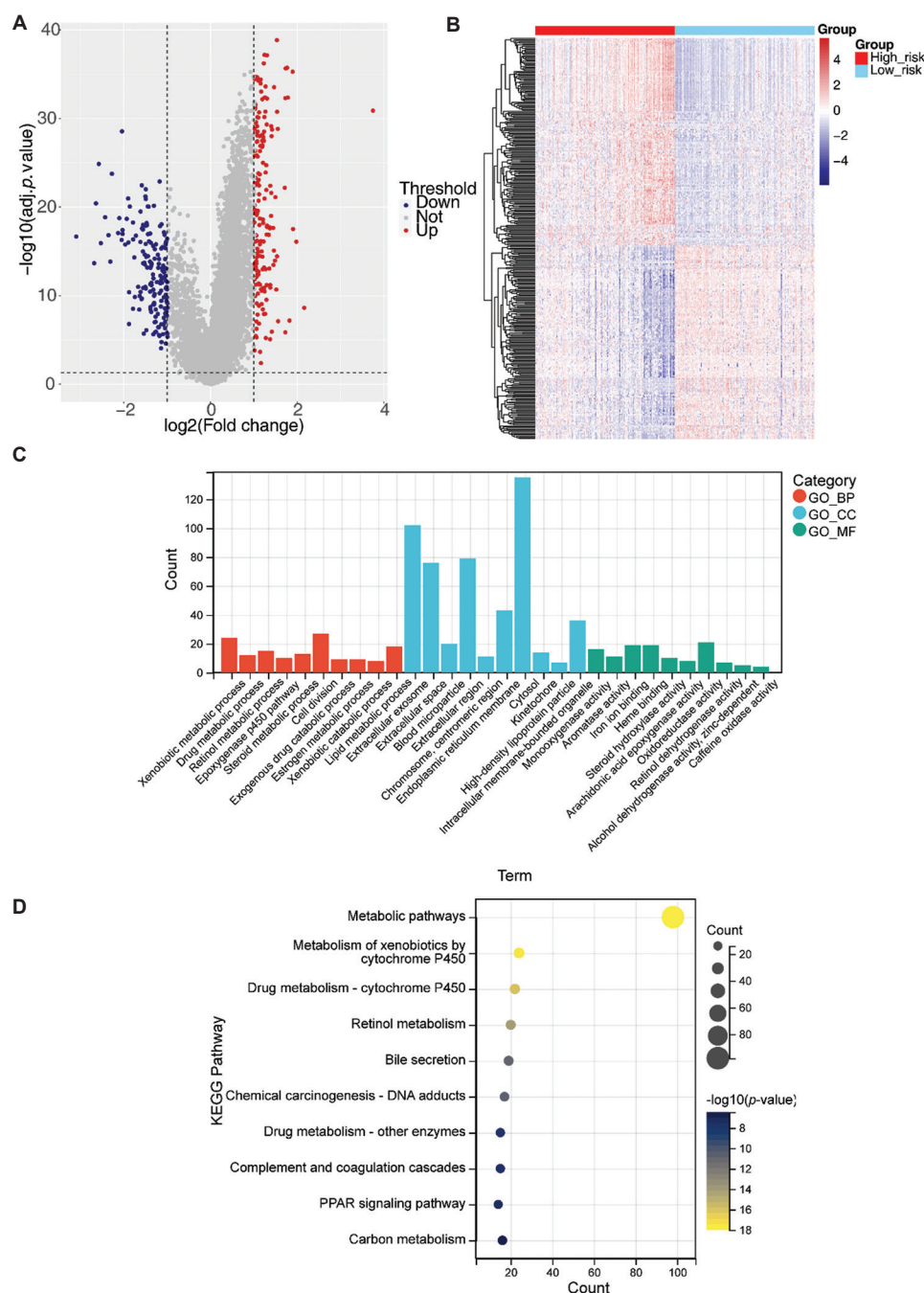


Figure 7. Comprehensive analysis of different risk groups. (A) Volcanic map of 352 differentially expressed genes (DEGs). A dot represents a gene, red dots represent genes with upregulated expression, blue dots represent genes with downregulated expression, and gray dots represent genes with non-significant expression differences. (B) Heat map of 352 DEGs between high- and low-risk groups using the Benjamini–Hochberg method for multiple test correction, the threshold was set as adjusted $p < 0.05$ and $|\log_2 \text{fold change}| > 1$. (C) Differential top 10 Gene Ontology Enrichment Map. The red column represents a biological process, the blue column represents a cellular component, and the green column represents a molecular function. (D) Kyoto Encyclopedia of Genes and Genomes enrichment plot of DEGs. The size of the dot represents the number of enriched genes.

series of rigorous experimental methods. Initially, western blotting was employed to verify the expression levels of the four selected biomarkers. The experimental results showed that the expression levels of KIF20A, SPP1, and TRNP1

were significantly upregulated in HCC tissues ($p < 0.05$), which was highly consistent with the conclusions drawn from bioinformatics analysis (Figure 10A). Among these biomarkers, TRNP1 exhibited the most significant and

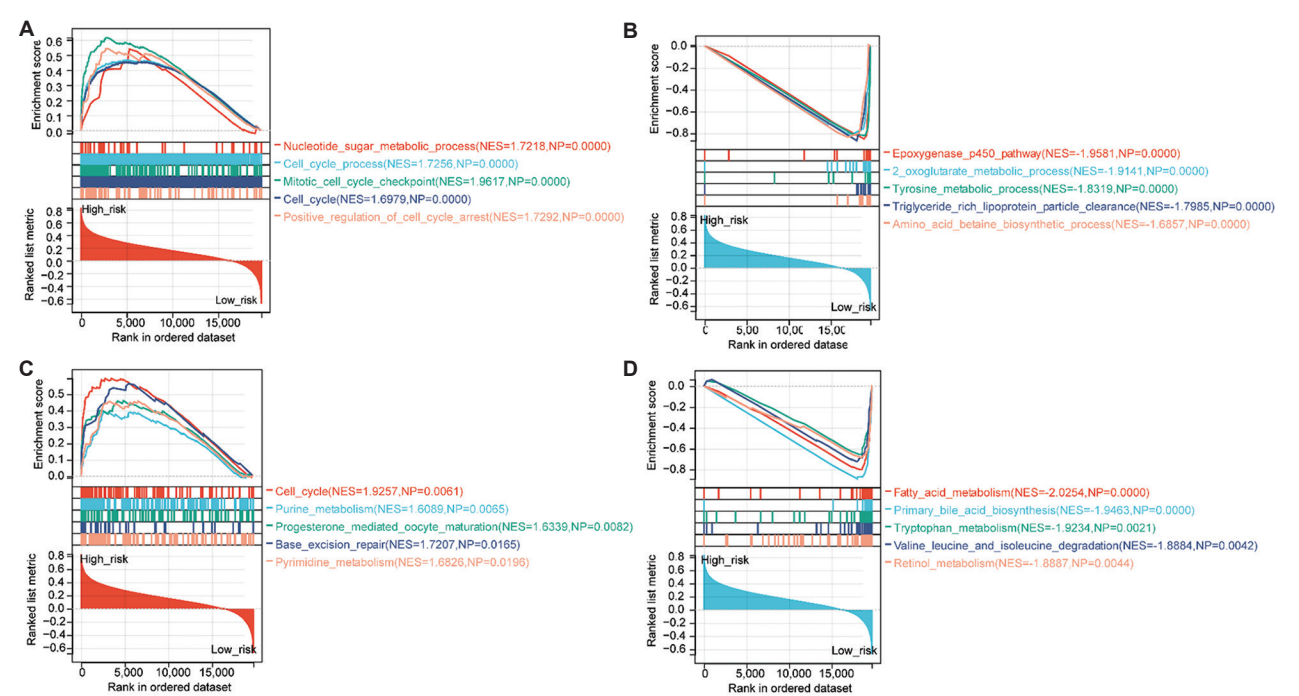


Figure 8. Gene set enrichment analysis of the two risk groups. Top five gene ontology biological process enrichment maps for (A) high-risk and (B) low-risk groups. Top five Kyoto Encyclopedia of Genes and Genomes enrichment maps for (C) high-risk and (D) low-risk groups. The lines of each color in the upper part of the figure represent a pathway, while the small vertical bars in the lower part represent the genes covered by each pathway. The significant enrichment threshold was set to |normalized enrichment score| > 1 and nominal *p*-value (NP) < 0.05.

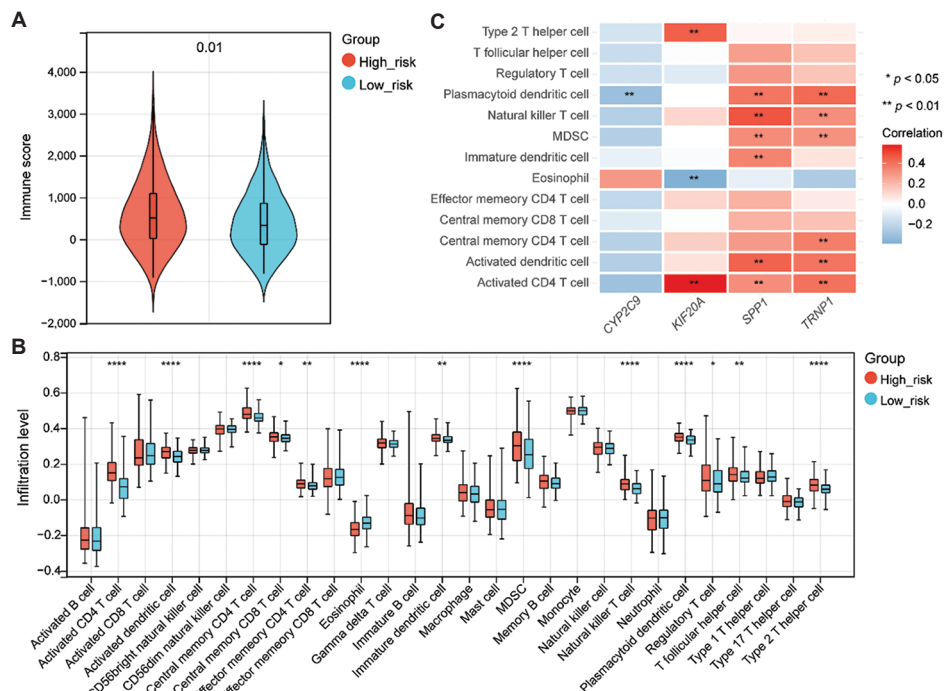


Figure 9. Immune-related analysis in different risk groups. (A) Violin plot of the immune scores in the high- and low-risk groups. (B) Boxplots for the infiltration levels of 28 immune cells between the groups. (C) Correlation heatmap between the differential existence of immune cells and four biomarkers. Red represents a positive correlation, and blue represents a negative correlation. The color intensity shows the correlation, with darker colors indicating a stronger correlation. Notes: * indicates *p* < 0.05; ** indicates *p* < 0.01; **** indicates *p* < 0.0001.

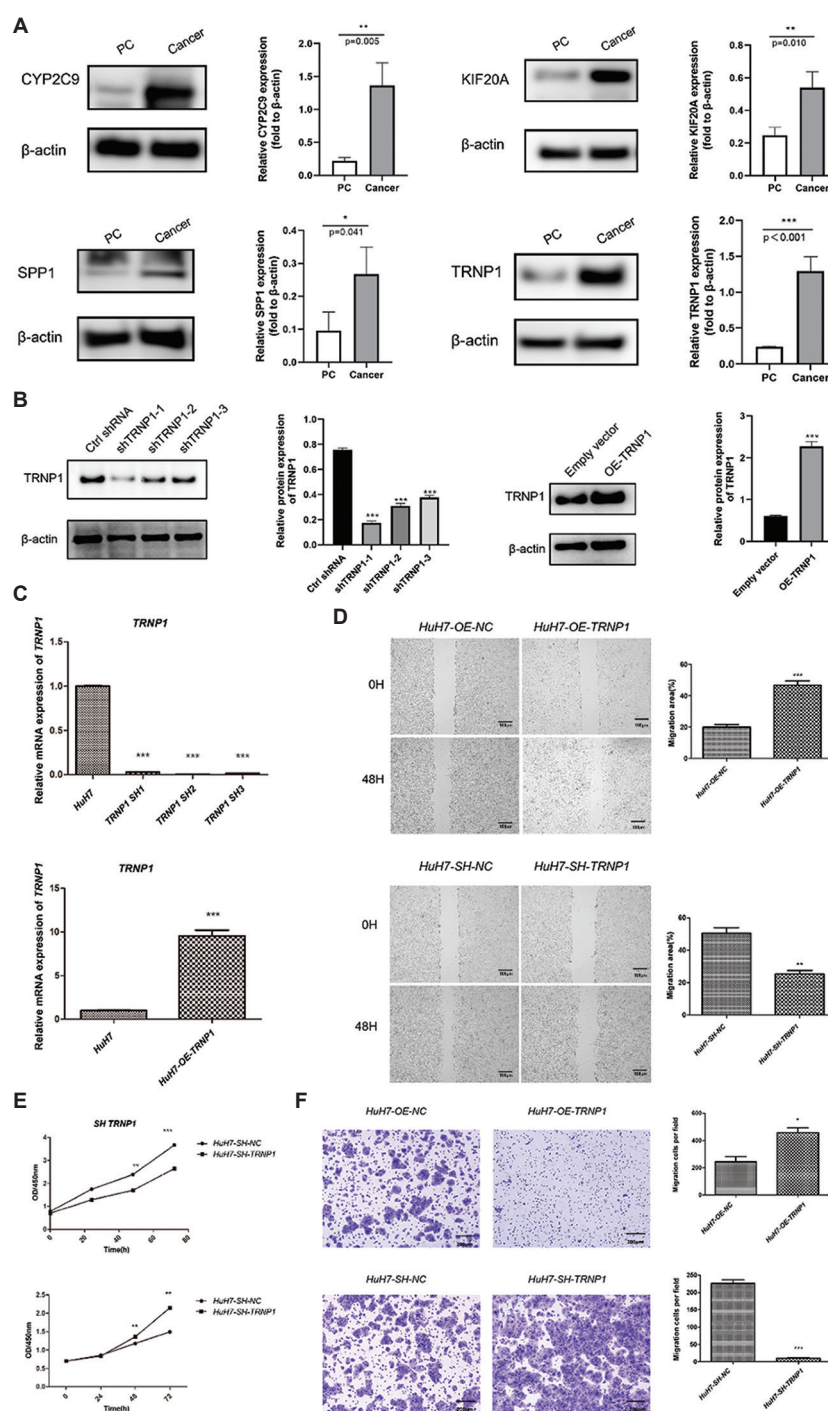


Figure 10. Experimental validation of biomarkers and investigation of the function of TMF-regulated nuclear protein 1 (TRNP1). (A) Relative expression of four biomarkers (cytochrome P450 family 2 subfamily C member [CYP269], kinesin family member 20A [KIF20A], secreted phosphoprotein 1 [SPP1], and TRNP1) at the protein level between the hepatocellular carcinoma (HCC) and peritumoral tissue samples. (B) Western blotting was used to assess the expression levels of TRNP1 in the *TRNP1* knockdown (*TRNP1*-1 ~ 3) and overexpression groups (OE) (HuH7-OE-*TRNP1*). (C) Real-time quantitative polymerase chain reaction was used to verify the expression levels of *TRNP1* in the *TRNP1* knockdown (short hairpin [Sh] *TRNP1*-SH1 ~ 3) and OE *TRNP1*. (D) The wound healing assay was employed to evaluate the migratory capacity of cells in both the *TRNP1* knockdown (HuH7-SH-*TRNP1*) and OE groups (HuH7-SH-*TRNP1*). Scale bar: 100 μ m, magnification: $\times 4$. (E) The cell counting kit-8 assay was used to evaluate the cell viability in both the *TRNP1* knockdown (HuH7-SH-*TRNP1*) and OE groups (HuH7-OE-*TRNP1*). (F) The Transwell invasion assay was used to evaluate the cell invasion ability in both the *TRNP1* knockdown (HuH7-SH-*TRNP1*) and OE groups (HuH7-OE-*TRNP1*). Scale bar: 200 μ m, magnification: $\times 10$.

Notes: * indicates $p < 0.05$; ** indicates $p < 0.01$; *** indicates $p < 0.001$.

highest upregulation ($p < 0.001$) in HCC tissues. Based on this finding, two techniques – gene knockdown and overexpression – were further utilized to explore the mechanisms of *TRNP1* in HCC. The results from RT-qPCR and western blotting showed that in the *TRNP1* knockdown group, the expression level of *TRNP1* was significantly downregulated, whereas, in the *TRNP1* overexpression group, its expression level was significantly upregulated (Figure 10B and C). This indicated that the knockdown and overexpression cell lines constructed were stable and could be used for subsequent analyses. Raw western blot images are provided in Figure R1.

To further elucidate the crucial role of *TRNP1* in the onset and progression of HCC, we examined the effects of both upregulating and downregulating *TRNP1* expression on the function of HuH7 cells (Figure 10D-F). The results indicated that in the *TRNP1* overexpression group, the migration distance of cells significantly increased, and cell viability and invasion ability were notably enhanced ($p < 0.05$), suggesting that the high expression of *TRNP1* may promote the migration, invasion, and proliferative capacity of HCC cells. Conversely, in the *TRNP1* knockdown group, the migration distance of cells significantly decreased, and cell viability and invasion ability were notably reduced ($p < 0.01$), further confirming the essential role of *TRNP1* in HCC cells.

4. Discussion

TRPCs are a crucial superfamily of selective cation channels that play a central role in maintaining calcium homeostasis and signaling. These processes are vital for regulating the development and progression of cancer.³³ The genes encoding TRPC channels (referred to as TRPGs) are involved in the regulation of these channels. TRPGs have been closely linked to the development of hepatocellular carcinoma (HCC).³⁴ Given this, we utilized bioinformatics analyses to identify biomarkers related to the TRP pathway in HCC patients. Our results provide a solid theoretical foundation and offer valuable insights into the prognosis of HCC, particularly for TRPGs.

Through our research, we discovered four biomarkers: CYP2C9, KIF20A, SPP1, and *TRNP1*, and created a risk-prognosis model tailored for HCC. Among them, the western blotting results of KIF20A, SPP1, and *TRNP1* were consistent with the bioinformatics results, showing upregulated expression in HCC. CYP2C9, a prominent and vital drug-metabolizing enzyme, plays a crucial role in the metabolism of various carcinogens and medications. Intriguingly, its expression is reduced in HCC. KIF20A, a member of the kinesin family, is indispensable for chromosome transport during mitosis and cell division.

Research has shown that high expression of KIF20A in HCC is linked to poor OS.³⁵ Furthermore, cellular experiments have identified hsa-miR-128-3p as a pivotal regulator of cell division in human hepatocytes, specifically targeting KIF20A.³⁶ Studies conducted by Lu *et al.*³⁶ have demonstrated abnormal expression of KIF20A in HCC tissues, with its expression levels potentially serving as an independent predictor of low OS and recurrence-free survival. Moreover, the downregulation of KIF20A has been proven to inhibit HCC proliferation both *in vivo* and *in vitro*,³⁷ underlining its importance as a key risk factor for HCC recurrence and survival. SPP1, another important biomarker, has been associated with the progression of various types of cancer. For example, SPP1 plays a role in the development of melanoma, and inhibitors targeting the bromodomain and extra-terminal motif can slow the progression of melanoma by influencing the atypical nuclear factor kappa B/secreted phosphoprotein 1 pathway.³⁸ In the context of castration-resistant prostate cancer, *SPP1* contributes to the activation of epithelial-mesenchymal transition through the phosphoinositide 3-kinase/protein kinase B and extracellular signal-regulated kinase 1/2 signaling pathways.³⁹ In addition, studies in mice have shown that blocking SPP1 or specifically deleting it in macrophages disrupts the structure of tumor-infiltrating B lymphocytes and enhances the sensitivity of HCC cells to immunotherapy.³⁹ These findings suggest that SPP1 may act as a negative prognostic factor for HCC. Furthermore, research has demonstrated that increased levels of SPP1 can stimulate the proliferation of HCC cells.⁴⁰ *TRNP1*, a low-complexity protein with the ability to undergo phase separation, is crucial for neural development, influencing neural stem cell self-renewal⁴¹ and brain folding.⁴² A study by Ren *et al.*⁴³ revealed that *TRNP1* is involved in lipid metabolism in HCC and is linked to the prognosis of the disease.⁴³ Notably, *TRNP1* is significantly upregulated in HCC,⁴² which was consistent with our experimental results. Experiments have shown that reducing the levels of *TRNP1* can induce apoptosis and senescence in HCC cells, thereby inhibiting tumor growth.⁴⁴ In this study, after the expression level of *TRNP1* was effectively knocked down, the migratory capacity, invasion ability, and viability of the cells significantly decreased. This suggested that downregulating the expression of *TRNP1* might potentially exert an inhibitory effect on the progression of HCC. These findings are consistent with our results and further strengthen the evidence supporting the role of these biomarkers in HCC.

The DEGs between the two risk groups were predominantly involved in a range of metabolic and signaling pathways. These include retinol metabolism, cell division, estrogen metabolism, lipid metabolism, bile secretion, peroxisome proliferator-activated receptor

signaling, and several others. Retinol, which is primarily stored in the liver, serves as a useful indicator of liver health. The levels of retinol in the serum, as well as those of its key precursor β -carotene, can provide insights into the status of the liver.⁴⁵ Intriguingly, studies have linked elevated retinol levels to the development of liver cancer.⁴⁶

Chen *et al.*⁴⁷ observed that as cancer stem cells become more aggressive, they undergo symmetrical cell division more frequently.^{48,49} In addition, the activation of cell cycle-related and estrogen signaling pathways, coupled with the suppression of lipid metabolism pathways, has been associated with a more favorable outcome in HCC.⁴⁹ Furthermore, studies have suggested that excessive growth hormone expression may contribute to the development of liver tumors.⁵⁰ Exosomes release microRNAs that play pivotal roles in tumor cell growth, blood vessel formation, and cancer metastasis within the tumor's surrounding environment. These microRNAs hold promise as diagnostic markers for identifying tumors.⁵¹ Bile acids, synthesized by the liver and modified by intestinal bacteria, are crucial for gut microbiota health, regulating lipid and carbohydrate metabolism, insulin sensitivity, and innate immune responses.⁵² Notably, there are gender-specific differences in the composition of gut microbiota and bile acids, which may explain the differing rates of liver cancer development between men and women.⁵³ In essence, these pathways are closely interconnected and significantly influence the progression of HCC.

In summary, we conducted a comprehensive analysis of the immune cells within the tumor's immune microenvironment. Notably, distinct differences were observed among 13 types of immune cells, particularly between activated CD4 T cells and dendritic cells, across various risk groups. Among these immune cells, *KIF20A* displayed the strongest positive correlation with activated CD4 T cells. The activation of tumor-specific CD4⁺ helper T cells is crucial for achieving effective anti-tumor immunity, and research has demonstrated that *KIF20A* can stimulate T-cell responses in transgenic mouse models.⁵⁴ Furthermore, *SPP1* plays a pivotal role in regulating macrophage polarization and enabling lung cancer to evade immune detection. Inhibition of *SPP1* has been shown to rejuvenate T-cell activation.⁵⁵ Intriguingly, *SPP1* expression levels also exhibit a positive correlation with the infiltration levels of dendritic cells, neutrophils, and macrophages in several types of cancer.⁵⁶ Therefore, it is reasonable to hypothesize that the prognostic genes may be associated with HCC through these immune cell populations.

5. Conclusion

In summary, we screened DE-TRPGs in HCC, obtained four biomarkers, and constructed a risk model, followed

by an immune microenvironment analysis and functional enrichment analysis of the model. Our study provides a theoretical basis and serves as a reference for the prognosis of HCC based on TRP pathway-related genes.

In this study, we used western blotting to verify the expression of biomarkers in HCC and its adjacent tissues. The results showed that the expression of CYP2C9 was different from the results of the dataset. This discrepancy may be caused by the small sample size, which may not accurately reflect the overall gene expression characteristics, so it is easy to produce results contrary to the actual trend. Moreover, sample heterogeneity is also a factor that should be acknowledged. The large differences among HCC patients (different etiologies, course of disease, and individual genetic background) may affect our PCR detection results, leading to a discrepancy with the expected expression trend. Notably, the expression trend of the data set is consistent with the existing literature. To address this issue and further validate the reliability of the existing results, we have planned to increase the sample size in subsequent studies. By expanding the sample size, the bias caused by the small sample size and heterogeneity could be reduced. This will allow the study results to more accurately reflect the true expression of genes in HCC, thus effectively verifying our research conclusions. In addition, in the future, we plan to conduct gene editing experiments, animal model construction, histopathological analysis, and other *in vivo* and *in vitro* experiments to further improve our research content and enhance the reliability of the conclusion.

Acknowledgments

We would like to acknowledge Professor Jiefeng He, whose expertise was invaluable in formulating the research questions and methodology.

Funding

None.

Conflict of interest

The authors declare that they have no competing interests.

Author contributions

Conceptualization: Dong Chen

Data curation: Jun Yin, Chao Yang, Bo Li

Investigation: Jing Li

Methodology: Jun Yin, Chao Yang, Bo Li

Software: Jun Yin, Chao Yang, Bo Li

Writing – original draft: Dong Chen

Writing – review & editing: Dong Chen

Ethics approval and consent to participate

The study was conducted in accordance with the Declaration of Helsinki and approved by the Shanxi Bethune Hospital Ethics Committee. Ethical approval number: SBQKL-2022-110. Informed consent was obtained from all subjects involved in the study.

Consent for publication

Written informed consent has been obtained from the patients to publish this paper.

Availability of data

The datasets analyzed in this study are available in the TCGA (<http://portal.gdc.cancer.gov/>) and ICGC (<https://dcc.icgc.org/>) databases, with reference codes TCGA-HCC and ICGC-HCC, respectively.

References

- Villanueva A. Hepatocellular carcinoma. *N Engl J Med*. 2019;380(15):1450-1462.
doi: 10.1056/NEJMr1713263.
- GBD 2017 Disease and Injury Incidence and Prevalence Collaborators. Global, regional, and national incidence, prevalence, and years lived with disability for 354 diseases and injuries for 195 countries and territories, 1990-2017: A systematic analysis for the global burden of disease study 2017. *Lancet*. 2018;392(10159):1789-1858.
doi: 10.1016/s0140-6736(18)32279-7
- Marengo A, Rosso C, Bugianesi E. Liver cancer: Connections with obesity, fatty liver, and cirrhosis. *Annu Rev Med*. 2016;67:103-117.
doi: 10.1146/annurev-med-090514-013832
- Kim DW, Talati C, Kim R. Hepatocellular carcinoma (HCC): Beyond sorafenib-chemotherapy. *J Gastrointest Oncol*. 2017;8(2):256-265.
doi: 10.21037/jgo.2016.09.07
- Zucman-Rossi J, Villanueva A, Nault JC, Llovet JM. Genetic landscape and biomarkers of hepatocellular carcinoma. *Gastroenterology*. 2015;149(5):1226-1239.e4.
doi: 10.1053/j.gastro.2015.05.061
- Ioannou GN. Epidemiology and risk-stratification of NAFLD-associated HCC. *J Hepatol*. 2021;75(6):1476-1484.
doi: 10.1016/j.jhep.2021.08.012
- Jemal A, Ward EM, Johnson CJ, *et al*. Annual report to the nation on the status of cancer, 1975-2014, featuring survival. *J Natl Cancer Inst*. 2017;109(9):djx030.
doi: 10.1093/jnci/djx030
- Fidler MM, Gupta S, Soerjomataram I, Ferlay J, Steliarova-Foucher E, Bray F. Cancer incidence and mortality among young adults aged 20-39 years worldwide in 2012: A population-based study. *Lancet Oncol*. 2017;18(12):1579-1589.
doi: 10.1016/s1470-2045(17)30677-0
- Bray F, Ferlay J, Soerjomataram I, Siegel RL, Torre LA, Jemal A. Global cancer statistics 2018: GLOBOCAN estimates of incidence and mortality worldwide for 36 cancers in 185 countries. *CA Cancer J Clin*. 2018;68(6):394-424.
doi: 10.3322/caac.21492
- Chimed T, Sandagdorj T, Znaor A, *et al*. Cancer incidence and cancer control in Mongolia: Results from the national cancer registry 2008-12. *Int J Cancer*. 2017;140(2):302-309.
doi: 10.1002/ijc.30463
- Forner A, Reig M, Bruix J. Hepatocellular carcinoma. *Lancet*. 2018;391(10127):1301-1314.
doi: 10.1016/s0140-6736(18)30010-2
- Zou J, Li H, Huang Q, *et al*. Dopamine-induced SULT1A3/4 promotes EMT and cancer stemness in hepatocellular carcinoma. *Tumour Biol*. 2017;39(10):1-10.
doi: 10.1177/1010428317719272.
- Grandhi MS, Kim AK, Ronnekleiv-Kelly SM, Kamel IR, Ghasebeh MA, Pawlik TM. Hepatocellular carcinoma: From diagnosis to treatment. *Surg Oncol*. 2016;25(2):74-85.
doi: 10.1016/j.suronc.2016.03.002
- Wu J, Liu W, Qiu X, *et al*. A noninvasive approach to evaluate tumor immune microenvironment and predict outcomes in hepatocellular carcinoma. *Phenomics*. 2023;3(6):549-564.
doi: 10.1007/s43657-023-00136-8
- Li JJ, Liang Q, Sun GC. Traditional Chinese medicine for prevention and treatment of hepatocellular carcinoma: A focus on epithelial-mesenchymal transition. *J Integr Med*. 2021;19(6):469-477.
doi: 10.1016/j.joim.2021.08.004
- Ran G, Feng XL, Xie YL, *et al*. The use of miR122 and its target sequence in adeno-associated virus-mediated trichostanthin gene therapy. *J Integr Med*. 2021;19(6):515-525.
doi: 10.1016/j.joim.2021.09.004
- Wang W, Wei C. Advances in the early diagnosis of hepatocellular carcinoma. *Genes Dis*. 2020;7(3):308-319.
doi: 10.1016/j.gendis.2020.01.014
- Hao X, Sun G, Zhang Y, *et al*. Targeting immune cells in the tumor microenvironment of HCC: New opportunities and challenges. *Front Cell Dev Biol*. 2021;9:775462.
doi: 10.3389/fcell.2021.775462
- Yuan L, Bing Z, Yan P, *et al*. Integrative data mining and meta-analysis to investigate the prognostic role of

- microRNA-200 family in various human malignant neoplasms: A consideration on heterogeneity. *Gene*. 2019;716:144025.
doi: 10.1016/j.gene.2019.144025
20. Schmitz C, Perraud AL, Johnson CO, *et al.* Regulation of vertebrate cellular Mg²⁺ homeostasis by TRPM7. *Cell*. 2003;114(2):191-200.
doi: 10.1016/s0092-8674(03)00556-7
 21. Shipston MJ. Ion channel regulation by protein S-acylation. *J Gen Physiol*. 2014;143(6):659-678.
doi: 10.1085/jgp.201411176
 22. Wang X, Li Y, Li Z, *et al.* Mitochondrial calcium uniporter drives metastasis and confers a targetable cystine dependency in pancreatic cancer. *Cancer Res*. 2022;82(12):2254-2268.
doi: 10.1158/0008-5472.Can-21-3230
 23. Delman KA. Introducing the “virtual tumor board” series in CA: A cancer journal for clinicians. *CA Cancer J Clin*. 2020;70(2):77.
doi: 10.3322/caac.21598
 24. Stoklosa P, Borgström A, Kappel S, Peinelt C. TRP channels in digestive tract cancers. *Int J Mol Sci*. 2020;21(5):1877.
doi: 10.3390/ijms21051877
 25. Li H. TRP channel classification. *Adv Exp Med Biol*. 2017;976:1-8.
doi: 10.1007/978-94-024-1088-4_1
 26. Julius D. TRP channels and pain. *Annu Rev Cell Dev Biol*. 2013;29:355-384.
doi: 10.1146/annurev-cellbio-101011-155833
 27. Xu J, Yang Y, Xie R, *et al.* The NCX1/TRPC6 complex mediates TGFβ-Driven migration and invasion of human hepatocellular carcinoma cells. *Cancer Res*. 2018;78(10):2564-2576.
doi: 10.1158/0008-5472.Can-17-2061
 28. Zhao F, Gao S, Qin X, *et al.* Comprehensive analysis of TRP channel-related genes for estimating the immune microenvironment, prognosis, and therapeutic effect in patients with esophageal squamous cell carcinoma. *Front Cell Dev Biol*. 2022;10:820870.
doi: 10.3389/fcell.2022.820870
 29. Ritchie ME, Phipson B, Wu D, *et al.* Limma powers differential expression analyses for RNA-sequencing and microarray studies. *Nucleic Acids Res*. 2015;43(7):e47.
doi: 10.1093/nar/gkv007
 30. Ito K, Murphy D. Application of ggplot2 to pharmacometric graphics. *CPT Pharmacometrics Syst Pharmacol*. 2013;2(10):e79.
doi: 10.1038/psp.2013.56
 31. Wilkerson MD, Hayes DN. ConsensusClusterPlus: A class discovery tool with confidence assessments and item tracking. *Bioinformatics*. 2010;26(12):1572-1573.
doi: 10.1093/bioinformatics/btq170
 32. Dennis G Jr., Sherman BT, Hosack DA, *et al.* DAVID: Database for annotation, visualization, and integrated discovery. *Genome Biol*. 2003;4(5):P3.
 33. Venkatachalam K, Montell C. TRP channels. *Annu Rev Biochem*. 2007;76:387-417.
doi: 10.1146/annurev.biochem.75.103004.142819
 34. Wang W, Liu P, Zhang Y, *et al.* Expression and functions of transient receptor potential channels in liver diseases. *Acta Pharm Sin B*. 2023;13(2):445-459.
doi: 10.1016/j.apsb.2022.09.005
 35. Jin Z, Peng F, Zhang C, Tao S, Xu D, Zhu Z. Expression, regulating mechanism and therapeutic target of KIF20A in multiple cancer. *Heliyon*. 2023;9(2):e13195.
doi: 10.1016/j.heliyon.2023.e13195
 36. Lu M, Huang X, Chen Y, *et al.* Aberrant KIF20A expression might independently predict poor overall survival and recurrence-free survival of hepatocellular carcinoma. *IUBMB Life*. 2018;70(4):328-335.
doi: 10.1002/iub.1726
 37. Shi C, Huang D, Lu N, *et al.* Aberrantly activated Gli2-KIF20A axis is crucial for growth of hepatocellular carcinoma and predicts poor prognosis. *Oncotarget*. 2016;7(18):26206-26219.
doi: 10.18632/oncotarget.8441
 38. Deng G, Zeng F, Su J, *et al.* BET inhibitor suppresses melanoma progression via the noncanonical NF-κB/SPP1 pathway. *Theranostics*. 2020;10(25):11428-11443.
doi: 10.7150/thno.47432
 39. Liu Y, Xun Z, Ma K, *et al.* Identification of a tumour immune barrier in the HCC microenvironment that determines the efficacy of immunotherapy. *J Hepatol*. 2023;78(4):770-782.
doi: 10.1016/j.jhep.2023.01.011
 40. Chen PF, Li QH, Zeng LR, *et al.* A 4-gene prognostic signature predicting survival in hepatocellular carcinoma. *J Cell Biochem*. 2019;120(6):9117-9124.
doi: 10.1002/jcb.28187
 41. Pang X, Zhang J, He X, *et al.* SPP1 promotes enzalutamide resistance and epithelial-mesenchymal-transition activation in castration-resistant prostate cancer via PI3K/AKT and ERK1/2 pathways. *Oxid Med Cell Longev*. 2021;2021:5806602.
doi: 10.1155/2021/5806602
 42. Esgleas M, Falk S, Forné I, *et al.* Trnp1 organizes diverse nuclear membrane-less compartments in neural stem cells.

- EMBO J.* 2020;39(16):e103373.
doi: 10.15252/embj.2019103373
43. Ren Z, Gao D, Luo Y, *et al.* Identification of fatty acid metabolism-related clusters and immune infiltration features in hepatocellular carcinoma. *Aging (Albany NY)*. 2023;15(5):1496-1523.
doi: 10.18632/aging.204557
 44. Wang HH, Chen WL, Cui YY, Gong HH, Li H. Cellular senescence throws new insights into patient classification and pharmacological interventions for clinical management of hepatocellular carcinoma. *World J Gastrointest Oncol*. 2023;15(9):1567-1594.
doi: 10.4251/wjgo.v15.i9.1567
 45. Arantes Ferreira Peres W, Villaça Chaves G, Saraiva Gonçalves JC, Ramalho A, Moraes Coelho HS. Assessment of the relative dose-response test as indicators of hepatic vitamin A stores in various stages of chronic liver disease. *Nutr Clin Pract*. 2013;28(1):95-100.
doi: 10.1177/0884533612455827
 46. Lai GY, Weinstein SJ, Albanes D, *et al.* Association of serum α -tocopherol, β -carotene, and retinol with liver cancer incidence and chronic liver disease mortality. *Br J Cancer*. 2014;111(11):2163-2171.
doi: 10.1038/bjc.2014.365
 47. Chen M, Lu C, Lu H, *et al.* Farnesoid X receptor via Notch1 directs asymmetric cell division of Sox9⁺ cells to prevent the development of liver cancer in a mouse model. *Stem Cell Res Ther*. 2021;12(1):232.
doi: 10.1186/s13287-021-02298-6
 48. Villa E. Role of estrogen in liver cancer. *Womens Health (Lond)*. 2008;4:41-50.
doi: 10.2217/17455057.4.1.41
 49. Gao S, Gang J, Yu M, Xin G, Tan H. Computational analysis for identification of early diagnostic biomarkers and prognostic biomarkers of liver cancer based on GEO and TCGA databases and studies on pathways and biological functions affecting the survival time of liver cancer. *BMC Cancer*. 2021;21(1):791.
doi: 10.1186/s12885-021-08520-1
 50. Messing A, Chen HY, Palmiter RD, Brinster RL. Peripheral neuropathies, hepatocellular carcinomas and islet cell adenomas in transgenic mice. *Nature*. 1985;316(6027):461-463.
doi: 10.1038/316461a0
 51. Li B, Cao Y, Sun M, Feng H. Expression, regulation, and function of exosome-derived miRNAs in cancer progression and therapy. *FASEB J*. 2021;35(10):e21916.
doi: 10.1096/fj.202100294RR
 52. Jia W, Xie G, Jia W. Bile acid-microbiota crosstalk in gastrointestinal inflammation and carcinogenesis. *Nat Rev Gastroenterol Hepatol*. 2018;15(2):111-128.
doi: 10.1038/nrgastro.2017.119
 53. Xie G, Wang X, Zhao A, *et al.* Sex-dependent effects on gut microbiota regulate hepatic carcinogenic outcomes. *Sci Rep*. 2017;7:45232.
doi: 10.1038/srep45232
 54. Yatsuda J, Irie A, Harada K, *et al.* Establishment of HLA-DR4 transgenic mice for the identification of CD4⁺ T cell epitopes of tumor-associated antigens. *PLoS One*. 2013;8(12):e84908.
doi: 10.1371/journal.pone.0084908
 55. Zhang Y, Du W, Chen Z, Xiang C. Upregulation of PD-L1 by SPP1 mediates macrophage polarization and facilitates immune escape in lung adenocarcinoma. *Exp Cell Res*. 2017;359(2):449-457.
doi: 10.1016/j.yexcr.2017.08.028
 56. Liu Y, Ye G, Dong B, *et al.* A pan-cancer analysis of the oncogenic role of secreted phosphoprotein 1 (SPP1) in human cancers. *Ann Transl Med*. 2022;10(6):279.
doi: 10.21037/atm-22-829